# Synthesis and Luminescent Properties of Novel Europium(III) Heterocyclic β-Diketone Complexes with Lewis Bases: Structural Analysis Using the Sparkle/AM1 Model

**Rani Pavithran,[a] M. L. P. Reddy,*[a] Severino A. Junior,[b] Ricardo O. Freire,[b] Gerd B. Rocha,[b] and Patricia P. Lima[b]**

**Keywords:** Europium / Lewis bases / Luminescence / O ligands / Sparkle/AM1 model

Tris(β-diketonato)europium(III) complexes of general formula $[Eu(TPI)_3{\cdot}L]$, with chelating ligands such as 3-phenyl-4-(4-toluoyl)-5-isoxazolone (HTPI) and adduct-forming reagents [L = $H_2O$, tri-*n*-octylphosphane oxide (TOPO), triphenylphosphane oxide (TPhPO), 1,10-phenanthroline], have been synthesized and characterized by elemental analysis and FT-IR, $^1H$ NMR, and photoluminescence spectroscopy. The coordination geometries of the complexes were calculated using the Sparkle/AM1 (Sparkle model for the calculation of lanthanide complexes within the Austin model 1) model. The ligand–$Eu^{3+}$ energy-transfer rates were calculated using a model of intramolecular energy transfer in lanthanide coordination complexes reported in the literature. The room-temperature PL spectra of the europium(III) complexes are composed of the typical $Eu^{3+}$ red emission, assigned to transitions between the first excited state ($^5D_0$) and the multiplet ($^7F_{0-4}$). The results clearly show that the substitution of water molecules by TOPO leads to greatly enhanced quantum yields (i.e., 1.3 % vs. 49.5 %) and longer $^5D_0$ lifetimes (220 vs. 980 μs). This can be ascribed to a more efficient ligand-to-metal energy transfer and a less efficient nonradiative $^5D_0$ relaxation process. The theoretical quantum yields are in good agreement with the experimental quantum yields, which highlights that the present theoretical approach can be a powerful tool for the a priori design of highly luminescent lanthanide complexes.
(© Wiley-VCH Verlag GmbH & Co. KGaA, 69451 Weinheim, Germany, 2005)

## Introduction

$Eu^{III}$ complexes have been regarded as attractive for use in electroluminescent devices for light-emitting diodes,[1,2] phosphors,[3] contrast agents for medical magnetic resonance imaging,[4] luminescent probes for analytes,[5] and light-emitting sensors in fluoroimmunoassays[6] because of their red emissions. The characteristic emissions of $Eu^{III}$ complexes mainly come from electric dipole transitions. Transition from the 4f inner shell of free $Eu^{III}$ is forbidden because it does not correlate with the change of parity. However, transitions that are forbidden by odd parity become partially allowed by mixing 4f and 5d states through ligand-field effects of designed $Eu^{III}$ complexes.[7] Unfortunately, the lanthanide ions are characterized by very low absorption coefficients ($\varepsilon < 1\ M^{-1}cm^{-1}$), which make direct excitation of the emitting levels impossible. Furthermore, coordination of solvent molecules to the lanthanide ions has dramatic effects on their excited state decay, because this decay is mainly governed by nonradiative processes. When solvents containing OH groups are coordinated to lanthanide ions, efficient nonradiative deactivations take place by vibronic coupling with the vibrational states of the OH oscillators.[8] A way to circumvent these difficulties is to use ligands bearing suitable chromophores that are capable of forming thermodynamically stable complexes with lanthanide ions. These ligands would play the antenna role, absorbing light and transferring excitation energy to the emitting ion. Additionally, when the $Ln^{3+}$ cation is coordinatively unsaturated by the original ligands, an additional neutral ligand coordinates to the lanthanide center to form a highly coordinated complex, thereby excluding the coordination of solvent molecules. Recently, a large number of highly coordinated complexes of lanthanide tris(β-diketonates) containing several nitrogen ligands such as 1,10-phenanthroline, 2,2′-bipyridine, and 2,2′:6′,6′′-terpyridine have been reported.[9,10] The central $Eu^{3+}$ ion coordinated with β-diketonato ligands gives stronger luminescence than that of the parent compounds, especially when β-diketonato ligands with aromatic or fluorinated substituents are present.[9] Phosphane oxide ligands in the europium(III) tris(β-diketonate) complex can produce a square-antiprismatic structure that promotes faster radiation rates and an increased quantum yield because of an increase in the $^5D_0$–$^7F_2$ emissions (electric dipole transitions), related to odd parity. Furthermore, increased quantum yields of the $Eu^{3+}$ complexes can be expected because coordination of the

[a] Chemical Sciences Division, Regional Research Laboratory (CSIR),
Thiruvananthapuram 695019, India
E-mail: mlpreddy@yahoo.co.uk
[b] Departmento de Química Fundamental – UFPE,
50670-901 Recife, PE, Brazil

phosphane oxide molecule prevents coordination of water or solvent molecule and lowers vibrations.[7] The above factors prompted us to utilize a novel heterocyclic β-diketone, namely 3-phenyl-4-(4-toluoyl)-5-isoxazolone, for the preparation of coordinatively saturated $Eu^{III}$ tris(isoxazolonate) complexes with Lewis bases such as trioctylphosphane oxide, triphenylphosphane oxide, or 1,10-phenanthroline (Figure 1). The synthesized $Eu^{3+}$ complexes have been characterized by various spectroscopic techniques and their photophysical properties investigated.

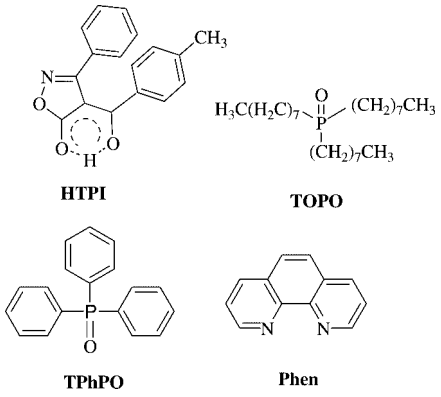


Figure 1. Structures of ligands used for the synthesis of $Eu^{III}$ complexes.

## Theoretical Approach

### Sparkle Model Geometries

The ground-state geometries of all $Eu^{III}$ complexes were calculated with the new version of the Sparkle/AM1 model[14] implemented in the MOPAC93r2 package.[15] The MOPAC keywords used in all Sparkle/AM1 calculations were: GNORM = 0.25, SCFCRT = 1.D-10 (in order to increase the SCF convergence criterion), and XYZ (the geometry optimizations were performed in Cartesian coordinates). Recently, Freire et al.[14] have improved the Sparkle model by presenting a much more accurate parameterization. This new parameterization, named Sparkle/AM1, yields an unsigned mean error for all interatomic distances between the $Eu^{3+}$ ion and the ligand atoms of the first sphere of coordination for 96 different $Eu^{3+}$ complexes of 0.09 Å, an improvement over the value of 0.28 Å for the second version SMLCII[16] and the value of 0.68 Å for the original version SMLC.[17]

### INDO/S-CI Electronic Structures

For all calculated ground-state geometries, we predicted their singlet and triplet excited states using the intermediate neglect of differential overlap/spectroscopic configuration interaction (INDO/S-CIS) method[18,19] implemented in the ZINDO program.[20] We used a point charge of +3e to represent the trivalent europium ion. The CIS space was gradually increased until there were no further meaningful changes in the calculated transitions. In contrast, the energy levels of the $Eu^{3+}$ metal ions were considered as being those of the free ion in the intermediate coupling scheme.[21] The INDO/S accuracy is about 1000 $cm^{-1}$.[18]

### Energy-Transfer Rates

According to the theoretical model developed by Malta et al.,[22,23] the following expression was obtained for the ligand–lanthanide ion energy-transfer (ET) rate, $W_{ET}$ [Equation (1)].

$$W_{ET} = W_{ET}^{mm} + W_{ET}^{em} \quad (1)$$

The first term, $W_{ET}^{mm}$, corresponds to the energy-transfer rate obtained from the multipolar mechanism and Equations (2) and (3)

$$W_{ET}^{mm} = W_{ET}^{mp} + W_{ET}^{dd} \quad (2)$$

$$\text{where } W_{ET}^{mp} = \frac{2\pi}{\eta}\frac{e^2 S_L}{(2J+1)G} F \sum_{\lambda} \gamma_{\lambda} \left\langle \alpha' J' \middle\| U^{(\lambda)} \middle\| \alpha J \right\rangle^2 \quad (3)$$

which correspond to the dipole–$2^{\lambda}$ pole mechanism ($\lambda$ = 2, 4, and 6), and Equation (4)

$$W_{ET}^{dd} = \frac{4\pi}{\eta}\frac{e^2 S_L}{(2J+1)G R_L^6} F \sum_{\lambda} \Omega_{\lambda}^{e,d} \left\langle \alpha' J' \middle\| U^{(\lambda)} \middle\| \alpha J \right\rangle^2 \quad (4)$$

corresponding to the dipole–dipole mechanism ($\lambda$ = 2, 4, and 6).

The second term of Equation (1), $W_{ET}^{em}$, corresponds to the energy-transfer rate obtained from the exchange mechanism. This term is calculated from Equation (5)

$$W_{ET}^{em} = \frac{8\pi}{3\eta}\frac{e^2 (1-\sigma_0)^2}{(2J+1)R_L^4} F \left\langle \alpha' J' \middle\| S \middle\| \alpha J \right\rangle^2 \sum_m \left| \left\langle \phi \middle| \sum_k \mu_Z(k)\, s_m(k) \middle| \phi' \right\rangle \right|^2 \quad (5)$$

In the above equations, $J$ represents the total angular momentum quantum number of the lanthanide ion, $G$ is the degeneracy of the ligand initial state, $a$ specifies a given 4f spectroscopic term, and $S_L$ is the electric dipole strength associated with the $\varphi \rightarrow \varphi'$ transition in the ligand. The quantities are reduced matrix elements $U^{(\lambda)}$, and $R_L$ is the distance from the lanthanide ion nucleus to the region of the ligand molecule in which the ligand donor (or acceptor) state is localized. In Equation (3), $S$ is the total spin operator of the lanthanide ion, $\mu_z$ is the $z$ component of the electric dipole operator and $s_m$ ($m$ = 0, ±1) is a spherical component of the spin operator, both for the ligand electrons, and $\sigma_0$ is a distance-dependent screening factor.

The quantities $F$ and $\gamma_{\lambda}$ are given by Equation (6)

 © 2005 Wiley-VCH Verlag GmbH & Co. KGaA, Weinheim 

$$F = \frac{1}{\eta\gamma_L}\sqrt{\frac{\ln 2}{\pi}}\,exp\left[-\left(\frac{\Delta}{\eta\gamma_L}\right)^2 \ln 2\right] \quad (6)$$

where $\gamma_L$ is the ligand-state band width at half-height and $\Delta$ is the difference between the donor and acceptor transition energies involved in the transfer process [Equation (7)].

$$\gamma_\lambda = (\lambda+1)\frac{\langle r^\lambda\rangle^2}{(R_L^{\lambda+2})^2}\langle 3\|C^{(\lambda)}\|3\rangle^2(1-\sigma_\lambda)^2 \quad (7)$$

where $\langle r^2\rangle$ is the radial expectation value of $r^\lambda$ for 4f electrons, $\langle 3\|C^{(2)}\|3\rangle$ is a reduced matrix element of the Racah tensor operator $C^{(\lambda)}$,[24] and the $\sigma_\lambda$ values are screening factors due to the 5s and 5p filled sub-shells of the lanthanide ion.

The selection rules that can be derived from the above equations are the following: $J + J' \geq \lambda \geq |J - J'|$, for the mechanisms expressed by Equations (1) and (2), and $\Delta J = 0, \pm 1$, for the exchange mechanism; in both cases $J' = J = 0$ is excluded. From the ligand side, the selection rules can be derived from the electric dipole strength, $S_L$, and the matrix element of the coupled operators $\mu_z$ and $S_m$ in Equation (3). The theoretical procedures for using the above equations and the corresponding selection rules have been discussed in detail elsewhere.[25]

The numerical solution of the rate equations describing the kinetics of the 4f–4f luminescence was carried out according to this model.[23] These numerical solutions of the rate equations yield the time dependence of the energy level populations, which reach the steady-state regime after $10^{-6}$–$10^{-5}$ s. These steady-state populations were then used to calculate the emission quantum yield, which is given by Equation (8)

$$q = \frac{A_T\eta_2}{\phi\eta_1} \quad (8)$$

where the subscripts 1 and 2 indicate the ground state and the emitting level ($^5D_0$), respectively, in the complex, $A_T$ is the sum of the coefficients of spontaneous emission for the $^5D_0 \rightarrow {}^7F_{0,1,2,4}$ transitions, and $\varphi$ is the pumping rate.

The microanalyses of complexes **1**–**4** show that the $Eu^{3+}$ ion has reacted with 3-phenyl-4-(4-toluoyl)-5-isoxazolone in a metal/ligand molar ratio of 1:3. The IR spectrum of complex **1** shows a broad absorption in the region 3000–3500 $cm^{-1}$, which indicates the presence of $H_2O$ molecules in the complex. The existence of water molecules in lanthanide complexes with heterocyclic β-diketones such as 4-acyl-3-methyl-1-phenylpyrazolones is well documented.[26,27] The presence of water molecules was also noticed in the complexes **3** and **4**. The disappearance of the broad band in the region 3000–3500 $cm^{-1}$ for complex **2**, which is associated with the coordinated water molecules in the neat complex **1**, suggests that water molecules have been displaced by the insertion of TOPO as a coordinating unit. The carbonyl stretching frequency of 3-phenyl-4-(4-toluoyl)-5-isoxazolone (1706 $cm^{-1}$) is shifted to lower wavenumbers in complexes **1**–**4** (1640 $cm^{-1}$ in **1**, 1643 $cm^{-1}$ in **2**, 1679 $cm^{-1}$ in **3**, and 1639 $cm^{-1}$ in **4**), thus indicating the involvement of the carbonyl oxygen atom in the complex formation with $Eu^{3+}$. Further, a shift in the P=O stretching frequency of the phosphane oxide molecules in complexes **2** (from 1143 to 1132 $cm^{-1}$) and **3** (from 1182 to 1155 $cm^{-1}$) shows the involvement of the phosphoryl oxygen atom in complex formation with $Eu^{3+}$. Vibration bands at 1608, 1574, 1476, 1445, and 1384 $cm^{-1}$ in complex **4** are characteristic of 1,10-phenanthroline.

The $^1H$ NMR spectrum of complex **1** shows all expected signals for the 3-phenyl-4-(4-toluoyl)-5-isoxazolone protons. The integration of the bands is in accordance with the proposed formula. A clear indication of complex formation is given by the absence of the enolic OH peak of the free ligand HTPI. Signals for water protons were also noticed in the complex **1**, as evidenced from the IR spectroscopic data. The signals of the phenyl protons are shifted upfield upon coordination with the metal ion in the complex (from $\delta$ = 6.93–7.36 ppm in HTPI to $\delta$ = 4.99–6.57 ppm in **1**). The signal of the $CH_3$ group in the HTPI complex is also shifted upfield (from $\delta$ = 2.31 ppm in HTPI to $\delta$ = 2.13 ppm in **1**) upon coordination with $Eu^{3+}$.

Figures 2, 3, 4, and 5 show the optimized molecular structures of the $Eu^{III}$ complexes **1**–**4**, respectively, obtained using the Sparkle/AM1 model. The $Eu^{3+}$ ion in complexes **1**, **3**, and **4** is nine-coordinate and the coordination polyhedron can be approximately described as a tricapped trigonal prism. On the other hand, the $Eu^{3+}$ ion in complex **2** is eight-coordinate and the coordination polyhedron can be described as a square antiprism. The spherical coordinates on the bonded oxygen atoms with respect to a coordinate system centered around the $Eu^{3+}$ ion are given in Tables 1 and 2. These structural data are consistent with a very low symmetry of the chemical environment around the $Eu^{3+}$ ion. An interesting point that is predicted by the present structure optimization is that the TOPO oxygen atoms are considerably closer to the $Eu^{3+}$ ion than the $H_2O$ oxygen atoms in the case of the hydrated compound **1**. Further, the two Eu–O bonds with TOPO ligands (2.32 and 2.33 Å) are shorter than the six Eu–O bonds with HTPI ligands (2.40–2.42 Å), as observed in the X-ray single-crystal structure (Eu–O bonds with TPhPO ligands: 2.31–2.32 Å; Eu–O bonds with hexafluoroacetylacetone ligand: 2.39–2.44 Å) of the complex tris-(hexafluoroacetylacetonato)europium(III) with phosphane oxide.[7] This clearly highlights that TOPO ligands interact more strongly with the $Eu^{3+}$ ion in complex **2**. Similarly, the TPhPO oxygen atoms are also found to be closer to the $Eu^{3+}$ ion than those of the water molecules in the hydrated complex. Another interesting phenomenon observed from the Sparkle/AM1 model prediction data for complex **4** is that the phenanthroline nitrogen atoms (Eu–N: 2.52 Å) are considerably further away from the $Eu^{3+}$ ion than the HTPI oxygen atoms. This is again in good agreement with the recently reported X-ray single-crystal data

 © 2005 Wiley-VCH Verlag GmbH & Co. KGaA, Weinheim 

for the complex [Eu(HFNH)$_3$] with phenanthroline [Eu–N: 2.59 and 2.61 Å; Eu–O bonds with 4,4,5,5,6,6,6-heptafluoro-1-(2-naphthyl)hexane-1,3-dione (HFNH): 2.34–2.40 Å].[28]

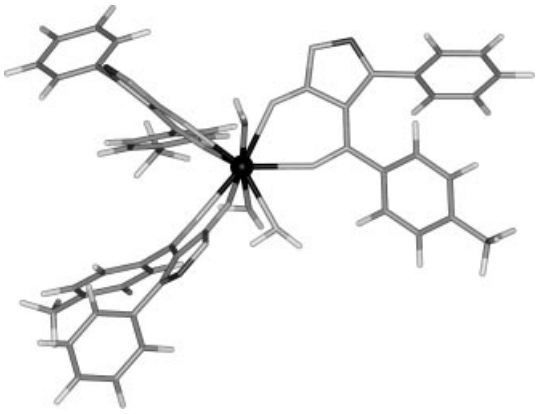

Figure 2. Optimized molecular structure of [Eu(TPI)$_3$·3H$_2$O] obtained from the Sparkle/AM1 model.

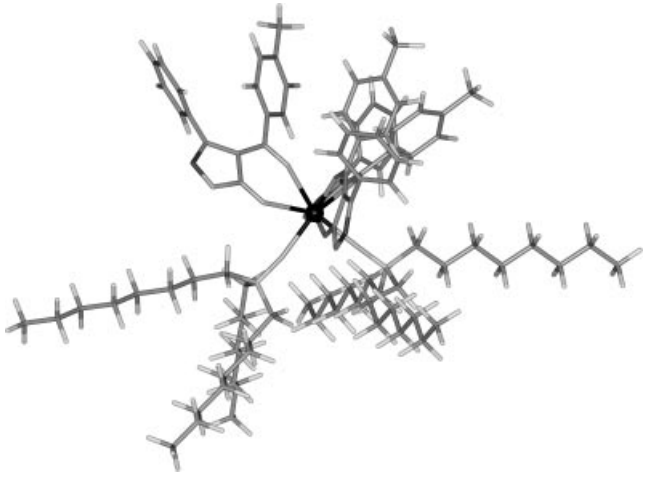

Figure 3. Optimized molecular structure of [Eu(TPI)$_3$·2TOPO] obtained from the Sparkle/AM1 model.

The excitation spectrum of the $^5D_0$ emission of $Eu^{3+}$ in [Eu(TPI)$_3$·3H$_2$O] at 14 K is shown in Figure 6. It consists of two broad bands in the UV region, with maxima at 265, 325, and 387 nm, and 4f–4f excitation lines. The excitation spectrum suggests an efficient ligand-to-metal energy transfer, since the most intense feature is a broad band that corresponds to transitions populating ligand-centered excited states. The typical excitation spectrum of [Eu(TPI)$_3$·2TOPO] (**2**) at 300 K, depicted in Figure 7, exhibits a large, broad band between 270 and 400 nm, with a maximum around 294 nm, corresponding to ligand excitations. This strongly suggests an efficient sensitization process between the ligands and the metal ion, with the ligand unit acting as an antenna.

The room-temperature emission spectra of europium complexes **1**–**4** (in the solid state) are shown in Figures 8, 9, 10, and 11, respectively. Comparing the emission spectra of the complexes, a significant change in the profile and in the splitting of the $^5D_0 \rightarrow {}^7F_{0-4}$ transitions (essentially in the

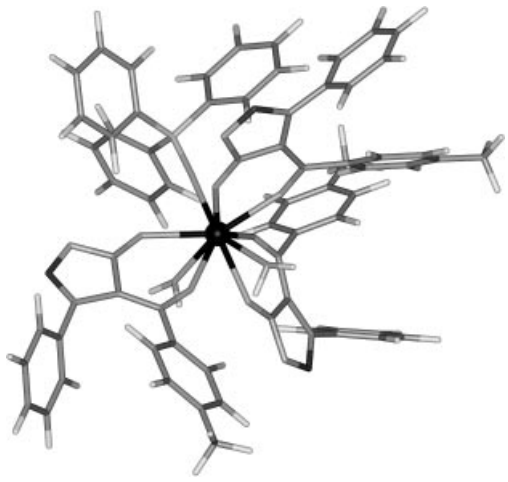

Figure 4. Optimized molecular structure of [Eu(TPI)$_3$·TPhPO·2H$_2$O] obtained from the Sparkle/AM1 model.

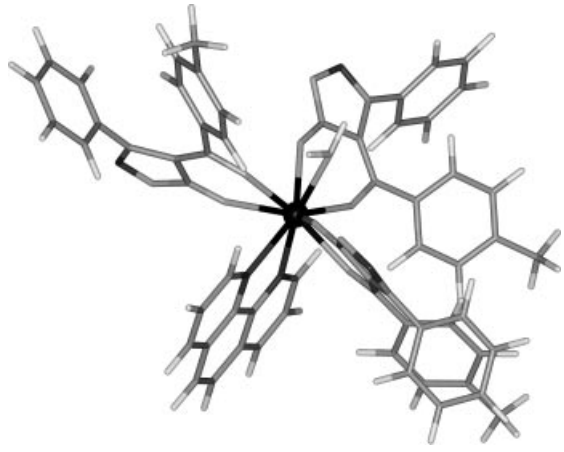

Figure 5. Optimized molecular structure of [Eu(TPI)$_3$·Phen·H$_2$O] obtained from the Sparkle/AM1 model.

Table 1. Spherical coordinates of the oxygen atoms bonded to the $Eu^{3+}$ ion in complexes **1** and **2**.

| Complex | Spherical coordinates | | |
|---|---|---|---|
| | $R$ [Å] | $\theta$ [°] | $\varphi$ [°] |
| **1** | 2.389 | 127.950 | 168.082 |
| HTPI oxygen atoms | 2.405 | 65.610 | 187.161 |
| | 2.403 | 75.196 | 101.320 |
| | 2.387 | 92.089 | 39.061 |
| | 2.407 | 59.321 | 295.129 |
| | 2.392 | 114.529 | 262.421 |
| H$_2$O oxygen atoms | 2.397 | 168.275 | 334.592 |
| | 2.393 | 10.984 | 113.529 |
| | 2.393 | 108.741 | 338.302 |
| **2** | 2.395 | 53.306 | 136.984 |
| HTPI oxygen atoms | 2.419 | 18.392 | 256.820 |
| | 2.401 | 108.903 | 74.190 |
| | 2.422 | 148.912 | 2.842 |
| | 2.398 | 132.205 | 159.055 |
| | 2.418 | 95.530 | 217.622 |
| TOPO oxygen atoms | 2.325 | 65.617 | 11.825 |
| | 2.318 | 98.986 | 288.886 |

 © 2005 Wiley-VCH Verlag GmbH & Co. KGaA, Weinheim 

Table 2. Spherical coordinates of the nitrogen and oxygen atoms bonded to the $Eu^{3+}$ ion in complexes **3** and **4**.

| Complex | Spherical coordinates | | |
|---|---|---|---|
| | $R$ [Å] | $\theta$ [°] | $\varphi$ [°] |
| **3** | 2.395 | 34.831 | 245.927 |
| HTPI oxygen atoms | 2.418 | 90.190 | 209.375 |
| | 2.418 | 70.557 | 325.000 |
| | 2.406 | 130.082 | 351.408 |
| | 2.413 | 70.863 | 127.890 |
| | 2.398 | 90.788 | 65.669 |
| TPhPO oxygen atom | 2.316 | 151.175 | 150.726 |
| $H_2O$ oxygen atoms | 2.403 | 101.427 | 269.854 |
| | 2.397 | 32.257 | 32.746 |
| **4** | 2.391 | 69.381 | 193.726 |
| HTPI oxygen atoms | 2.411 | 52.648 | 266.381 |
| | 2.414 | 89.858 | 125.151 |
| | 2.395 | 98.767 | 61.811 |
| | 2.413 | 125.792 | 253.769 |
| | 2.391 | 138.067 | 342.370 |
| N (Phen) | 2.520 | 22.017 | 85.750 |
| | 2.522 | 63.305 | 353.118 |
| $H_2O$ oxygen atom | 2.396 | 134.142 | 172.751 |

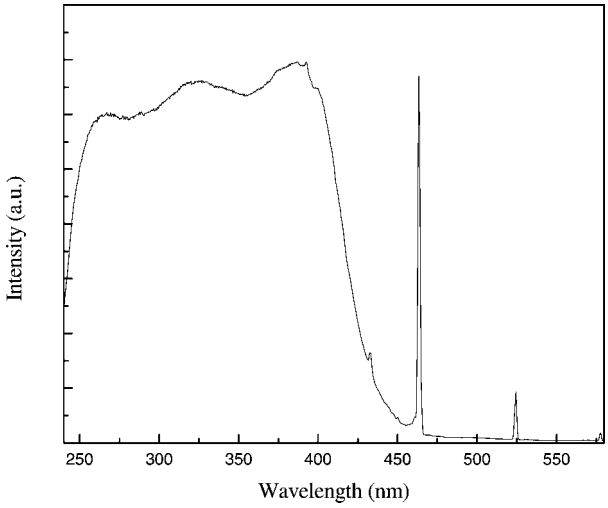


Figure 6. The excitation spectrum of $^5D_0$ emission ($\lambda_{em}$ = 614 nm) of $Eu^{3+}$ in $[Eu(TPI)_3{\cdot}3H_2O]$ (**1**) at 14 K.

$^5D_0 \rightarrow {}^7F_2$ lines) can be observed upon substitution of water molecules in **1** by Lewis bases such as TOPO, TPhPO, and Phen. The emission spectra of the complexes display characteristic sharp peaks in the 575–725 nm region associated with the $^5D_0 \rightarrow {}^7F_J$ transitions of the $Eu^{3+}$ ion. The five expected Stark components of the $^5D_0 \rightarrow {}^7F_{0-4}$ transitions are well resolved and the hypersensitive $^5D_0 \rightarrow {}^7F_2$ transition is very intense, pointing to a highly polarizable chemical environment around the $Eu^{3+}$ ion, and is responsible for the brilliant red emission color of these complexes.[29] The emission spectra of the complexes show only one peak for the $^5D_0 \rightarrow {}^7F_0$ transition, thus indicating the presence of a single chemical environment around the $Eu^{3+}$ ion, and also show that the $Eu^{3+}$ ion occupies a low symmetry site. Further, the emission band at 525 nm, corresponding to the emission from the lowest triplet state of the ligand, is not observed

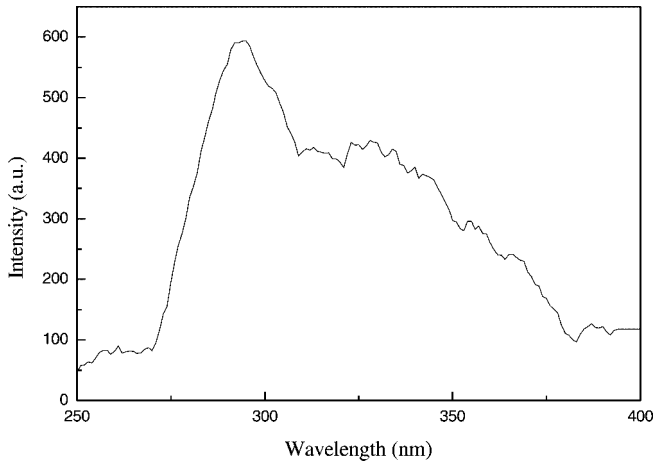


Figure 7. The excitation spectrum of $^5D_0$ emission ($\lambda_{em}$ = 614 nm) of $Eu^{3+}$ in $[Eu(TPI)_3{\cdot}2TOPO]$ (**2**) at 300 K.

in these $Eu^{3+}$ complexes, thus indicating that energy transfer from the lowest triplet state of 4-toluoyl-5-isoxazolone to the $Eu^{3+}$ ion is efficient.

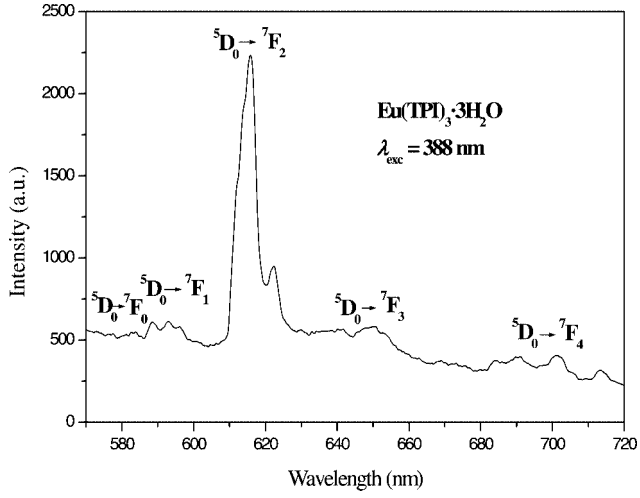


Figure 8. Room-temperature PL spectrum of compound **1** excited at 388 nm.

The experimental intensity parameters $\Omega_2$ and $\Omega_4$ were determined from the emission spectra (Figures 8–11) based on the $^5D_0 \rightarrow {}^7F_2$ and $^5D_0 \rightarrow {}^7F_4$ electronic transitions, respectively, and by expressing the emission intensity $I = \hbar\bar{\omega}A_{RAD}N$ in terms of the surface under the emission curve. Here $\hbar\bar{\omega}$ is the transition energy, $A_{RAD}$ is the corresponding coefficient of spontaneous emission, and $N$ is the population of the emitting level $^5D_0$. The magnetic dipole allowed $^5D_0 \rightarrow {}^7F_1$ transition was taken as the reference.[30,31] The $A_{RAD}$ values are given by Equation (9)[32]

$$A_{RAD} = \frac{4e^2\omega^3}{3\eta c^3}\chi\sum_{\lambda}\Omega_\lambda\left\langle {}^7F_J\left\|U^{(\lambda)}\right\|{}^5D_0\right\rangle^2\frac{1}{2J+1} \quad (9)$$

where, $\lambda$ = 2 and 4, $\chi$ is the Lorentz local field correction term that is given by $n(n^2 + 2)^2/9$, with a refraction index, $n$,

 © 2005 Wiley-VCH Verlag GmbH & Co. KGaA, Weinheim 

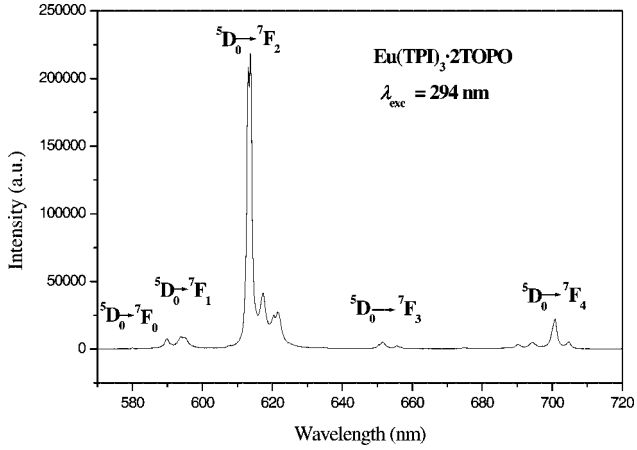


Figure 9. Room-temperature PL spectrum of compound **2** excited at 294 nm.

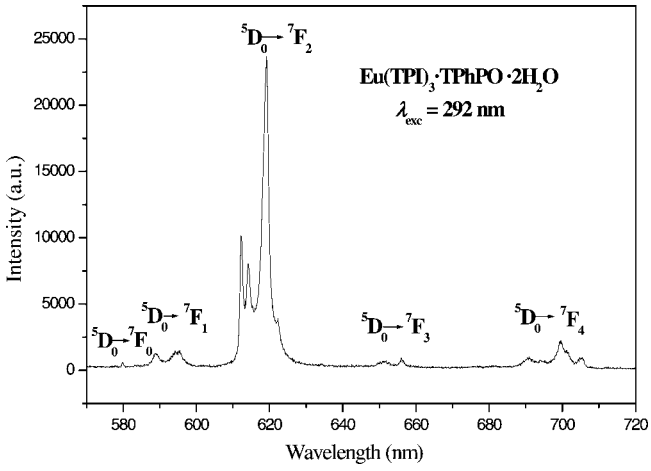


Figure 10. Room-temperature PL spectrum of compound **3** excited at 292 nm.

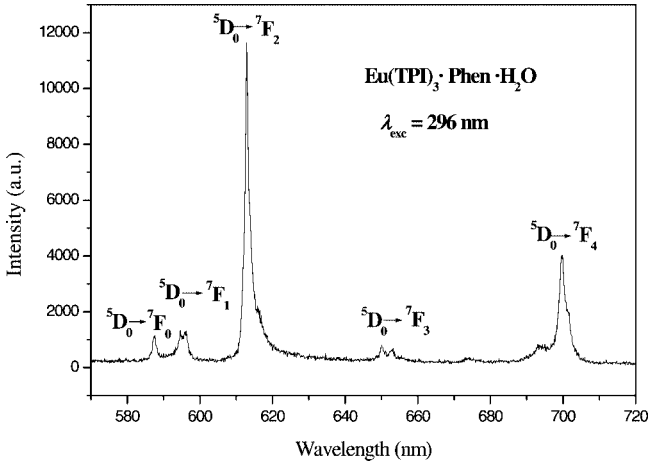


Figure 11. Room-temperature PL spectrum of compound **4** excited at 296 nm.

of 1.5, and $\langle {}^5D_0 \| U^{(2)} \| {}^7F_J \rangle^2$ are the squared reduced matrix elements whose values are 0.0032 and 0.0023 for $J = 2$ and 4, respectively.[21] Table 3 presents the values of $\Omega_2$ and $\Omega_4$ for complexes **1**–**4** at room temperature (300 K) and the values at 14 K for complex **1**. The high values of $\Omega_2$ for complexes **1**–**3** might be interpreted as a consequence of the hypersensitive behavior of the $^5D_0 \rightarrow {}^7F_2$ transition,[33] suggesting that dynamic coupling mechanism is quite operative in these complexes.

Table 3. Experimental intensity parameters, radiative ($A_{RAD}$) and nonradiative decay rates ($A_{NR}$), experimental ($q_{exp}$) and theoretical emission quantum yields ($q_{theo}$), $^5D_0$ lifetime ($\tau$), and quantum efficiency ($\varepsilon$) for complexes **1**–**4** at 300 K.

| | $\Omega_2$ ($\times 10^{-20}$) [cm$^2$] | $\Omega_4$ ($\times 10^{-20}$) [cm$^2$] | $A_{RAD}$ [s$^{-1}$] | $A_{NR}$ [s$^{-1}$] | $q_{exp}$ [%] | $q_{theo}$ [%] | $\tau$ [ms] | $\varepsilon$ [%] |
|---|---|---|---|---|---|---|---|---|
| **1** | 8.10 | 5.76 | 381 | 2952 | 1.3 | 10.80 | 0.30 | 13 |
| **1**[a] | 11.93 | 11.28 | 580 | 2277 | – | – | 0.35 | 20 |
| **2** | 20.72 | 6.42 | 773 | 242 | 49.5 | 52.53 | 0.98 | 76 |
| **3** | 17.55 | 5.76 | 658 | 1265 | 8.3 | 23.00 | 0.52 | 34 |
| **4** | 6.02 | 6.99 | 335 | 1304 | 5.5 | 14.02 | 0.61 | 20 |

[a] Measured at 14 K.

By comparing the values of the $\Omega_2$ parameter determined for the complexes at room temperature, it can be concluded that the polarizability is in the order [Eu(TPI)$_3$·Phen·H$_2$O] (**4**) < [Eu(TPI)$_3$·3H$_2$O] (**1**) < [Eu(TPI)$_3$·TPhPO·2H$_2$O] (**3**) and [Eu(TPI)$_3$·2TOPO] (**2**). As pointed out by Reisfeld and Jørgensen,[34] the intensity parameter $\Omega_2$ can be correlated to the degree of covalency experienced by the lanthanide ion, greater values being obtained in more covalent surroundings (e.g., $1.2 \times 10^{-20}$ cm$^2$ for $LaF_3$:Eu; $1 \times 10^{-19}$ cm$^2$ for $Y_2O_3$:Eu). Therefore, the high value of $\Omega_2$ obtained for complex **2** in the present investigations indicates that the covalent contribution is larger for the complex containing the TOPO ligand, which may be ascribed to stronger bonding. It can be argued that this is expected to increase the ligand–Eu$^{3+}$ ion energy-transfer rate,[35] since a stronger bond causes the ligand–metal ion distances to be shorter, thus increasing electric-dipole interactions and wavefunction overlap.

The lifetime values ($\tau$) of the $^5D_0$ level were determined from the luminescence decay profiles for the complexes at room temperature by fitting with a mono-exponential curve; they are listed in Table 3. The relatively shorter lifetimes obtained for complex **1** may be due to dominant nonradiative decay channels associated with vibronic coupling due to the presence of water molecules, as has been documented in many hydrated europium β-diketonate complexes.[25] A longer lifetime value has been observed for complex **2** as compared to complexes **3** and **4**. This may also be due to the presence of water molecules in complexes **3** and **4**.

The nonradiative rates, $A_{NR}$, can be obtained from the calculated $A_{RAD}$ rates and the experimental decay rates by Equation (10).[35]

$$\tau^{-1} = A_T = A_{RAD} + A_{NR} \quad (10)$$

It is clear from Table 3 that complexes **1**, **3**, and **4**, which have water molecules in the coordination sphere, exhibit lower quantum efficiencies and lifetimes. This is due to the

 © 2005 Wiley-VCH Verlag GmbH & Co. KGaA, Weinheim 

presence of O–H oscillators in these systems, which effectively quench the luminescence of the $Eu^{3+}$ ion. On the other hand, complex **2**, which does not contain any water molecule in its coordination sphere, as is also evident from the molecular structure analysis with the Sparkle/AM1 model, exhibits high quantum efficiency and lifetime values. The experimental and theoretical quantum yields of these complexes increase in the order **1** < **4** < **3** < **2**. The theoretical quantum yield of complex **2** is in good agreement with the experimental value. On the other hand, the degree of agreement between the theoretical and experimental quantum yields in the case of **1**, **3**, and **4** is not promising. This may be due to the fact that the model for quantum yield does not take into account the suppression by vibronic coupling with coordinated water molecules. Another factor contributing towards the error could be the phenomenon of nonradiative deactivation via a charge-transfer state involving the metal and the ligand.

The energy-transfer rates from the ligand triplet state T to the $^5D_1$ and $^5D_0$ levels and energy-transfer rates from the singlet state S to the $^5D_4$ level are presented in Table 4. We assumed a singlet→triplet intersystem crossing rate of $10^8$ $s^{-1}$, a triplet state decay rate of $10^5$ $s^{-1}$, and a nonradiative decay rate of $10^6$ $s^{-1}$.[9] The theoretical energies of the singlet and triplet were used in the calculation of the energy-transfer rates. We considered an average of the three singlet and triplet excited states where the difference of the energy between the average values of the triplet states of the $^5D_J$ levels is smaller than 9.000 $cm^{-1}$. The average values of the singlet excited states were chosen because these values are closer to the values of the experimental singlet excited state of the complexes. The values for the theoretical triplet excited states were also chosen in the same way. An energy level diagram for the compound [$Eu(TPI)_3$·2TOPO] is shown in Figure 12. The symbols $S_0$, T, and $S_1$ shown in Figure 12 refer to the ground singlet, lowest energy triplet, and first excited singlet, respectively. The theoretical energies of the singlet and triplet were used in this diagram.

Table 4. Predicted values of intramolecular energy-transfer rates in compounds **1**–**4**. The back transfer rates were calculated by multiplying the direct transfer rates by the Boltzmann factor $e^{-|\Delta|/kT}$ at room temperature.

| Compound | Levels | Transfer rate [$s^{-1}$] | Back transfer rate [$s^{-1}$] |
|---|---|---|---|
| **1** | $S_1 \rightarrow {}^5D_4$ | $1.386 \times 10^5$ | $1.924 \times 10^{-5}$ |
| | $T \rightarrow {}^5D_1$ | $3.933 \times 10^8$ | $3.400 \times 10^{-1}$ |
| | $T \rightarrow {}^5D_0$ | $8.353 \times 10^7$ | $9.757 \times 10^{-6}$ |
| **2** | $S_1 \rightarrow {}^5D_4$ | $7.698 \times 10^4$ | $8.703 \times 10^{-8}$ |
| | $T \rightarrow {}^5D_1$ | $1.703 \times 10^8$ | $4.121 \times 10^{-4}$ |
| | $T \rightarrow {}^5D_0$ | $2.541 \times 10^7$ | $8.298 \times 10^{-9}$ |
| **3** | $S_1 \rightarrow {}^5D_4$ | $4.311 \times 10^4$ | $7.148 \times 10^{-9}$ |
| | $T \rightarrow {}^5D_1$ | $1.028 \times 10^8$ | $1.738 \times 10^{-5}$ |
| | $T \rightarrow {}^5D_0$ | $1.306 \times 10^7$ | $2.982 \times 10^{-10}$ |
| **4** | $S_1 \rightarrow {}^5D_4$ | $6.757 \times 10^5$ | $5.010 \times 10^{-1}$ |
| | $T \rightarrow {}^5D_1$ | $1.169 \times 10^8$ | $7.086 \times 10^{-5}$ |
| | $T \rightarrow {}^5D_0$ | $1.604 \times 10^7$ | $1.313 \times 10^{-9}$ |

According to the selection rules for the process of energy transfer, in the case of the ion $Eu^{3+}$, levels $^5D_2$, $^5L_6$, $^5G_6$, and $^5D_4$ are good candidates for the multipolar mechanism, while for the exchange mechanism a strong candidate is level $^5D_1$.[36] Therefore for the complexes in this work, the predominant process in the transfer of energy is the exchange mechanism. In accordance with Table 4, the values of the energy-transfer rate indicate that the energy transfer is predominant from the triplet state of the ligand to the $^5D_1$ and $^5D_0$ levels of the $Eu^{3+}$ ion.

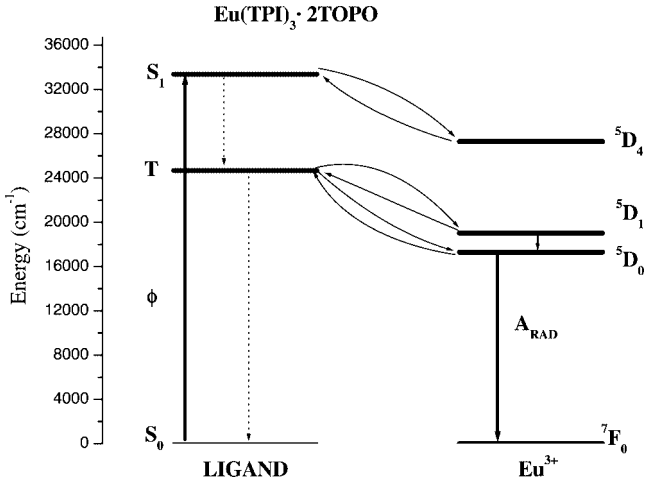


Figure 12. The energy level diagram of ligands and $Eu^{3+}$ ion in [$Eu(TPI)_3$·2TOPO].

## Conclusions

In the present study, various new 3-phenyl-4-(4-toluoyl)-5-isoxazolonate complexes of $Eu^{3+}$ with Lewis bases such as tri-*n*-octylphosphane oxide, triphenylphosphane oxide, and 1,10-phenanthroline have been synthesized and characterized by various spectroscopic techniques. Their ground-state geometries have been calculated using the Sparkle/AM1 model. Experimental and theoretical results on ligand-field parameters, 4f–4f intensities, and intramolecular energy-transfer processes have been described. The photophysical properties of the above complexes have been determined and compared with the theoretical predictions.

The characteristic emission spectra of $Eu^{3+}$ complexes **1**–**4** show a very high intensity for the hypersensitive $^5D_0 \rightarrow {}^7F_2$ transition, pointing to a highly polarizable chemical environment around the $Eu^{3+}$ ion. The theoretically predicted values of intramolecular energy-transfer rates of complexes **1**–**4** clearly indicate that the energy transfer is predominant from the triplet state of the ligand to the $^5D_1$ and $^5D_0$ levels of the $Eu^{3+}$ ion. Higher quantum yields (49.5%) and lifetime values (980 μs) are observed for complex **2** than for complexes **1**, **3**, and **4**, and this can be ascribed to a more efficient ligand-to-metal energy transfer and less efficient nonradiative $^5D_0$ relaxation process in the former case. This is also in accordance with the strong coordination between the oxygen atom of TOPO and the $Eu^{3+}$ ion, as predicted by the Sparkle model. It is also important to point out that there is a good agreement between the experimental and the theoretical quantum yields, especially for complex **2**, thus

 © 2005 Wiley-VCH Verlag GmbH & Co. KGaA, Weinheim 

showing that the theoretical estimation of quantum yields can be a valuable tool for developing efficient light conversion molecular devices (LCMDs). The luminescent properties observed in the Eu–heterocyclic β-diketonate complexes indicate that 3-phenyl-4-aroyl-5-isoxazolones form a promising class of antenna molecules that can be employed in the design of new LCMDs.

## Experimental Section

**Materials and Methods:** The commercially available chemicals europium(III) nitrate hexahydrate, 99.9% (Acros Organics); 3-phenyl-5-isoxazolone, 98% (Aldrich), 4-toluoyl chloride, 98% (Aldrich), trioctylphosphane oxide, 99% (Aldrich), triphenylphosphane oxide, 98% (Aldrich), and 1,10-phenanthroline, 99.5% (Merck) were used without further purification. All the other chemicals used were of analytical reagent grade. C, H and N analyses were performed with a Perkin–Elmer Series 2 Elemental Analyser 2400. A Nicolet FT-IR 560 Magna Spectrometer (KBr, neat) was used to obtain IR spectroscopic data and a Bruker 300 MHz NMR spectrometer was used to obtain $^1$H NMR spectra of the compounds in $CDCl_3$ or [$D_6$]acetone. Photoluminescence (PL) spectra were recorded with a Jobin Yvon Spex spectrometer (HR, 460) coupled to an R928 Hamamatsu photomultiplier. A Xe arc lamp (150 mW) coupled to a Jobin Yvon Spex monochromator (TRIAX 180) was used as the excitation source. All the spectra were corrected for the response of the detector. The lifetime measurements were taken using a pulsed Xe arc lamp (5 mJ/pulse, 3 ms bandwidth) coupled to a Kratos GM-252 monochromator and a Spex 1934 C phosphorimeter. The emission quantum yield, $q_x$, of the $^5D_0$ emission band of the $Eu^{III}$ complexes, defined as the ratio between the number of photons emitted by the $Eu^{3+}$ ion and the number of photons absorbed by the ligand, was determined from the following formula:

$$q_x = \left(\frac{1-r_{st}}{1-r_x}\right)\left(\frac{\Delta\Phi_x}{\Delta\Phi_{st}}\right)q_{st}$$

where $r_{st}$ and $r_x$ are the amounts of exciting radiation reflected by the standard phosphor and by the sample, respectively, and $q_{st}$ is the quantum yield of the standard phosphor. The terms $\Delta\Phi_x$ and $\Delta\Phi_{st}$ give the integrated photon flux (photons per second) for the sample and the standard phosphor, respectively. A detailed description of this method has been presented elsewhere.[11,12]

**Synthesis of 3-Phenyl-4-(4-toluoyl)-5-isoxazolone (HTPI):** A mixture of 3-phenyl-5-isoxazolone (3 g, 18 mmol), $Ca(OH)_2$ (2.7 g, 27 mmol), and dioxane (30 mL) was heated at 50 °C for 0.5 h. 4-Toluoyl chloride (2.88 g, 18 mmol) was then added dropwise and the mixture stirred for 6 h (Scheme 1). The crude product was filtered, dried, and recrystallized from ethyl acetate.[13] The synthesized 3-phenyl-4-(4-toluoyl)-5-isoxazolone was identified by elemental analyses and IR and $^1$H NMR spectroscopic data.

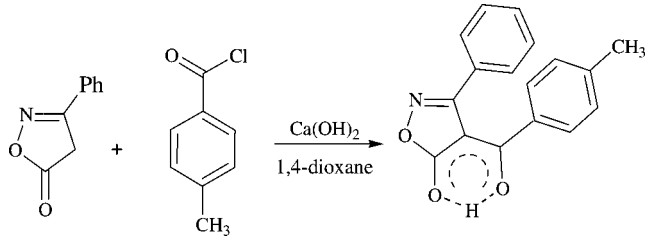


Scheme 1.

**HTPI:** M.p. 145 °C. $^1$H NMR: $\delta$ = 6.93–7.37 (m, 9 H, phenyl), 2.31 (3 H, methyl) ppm. The peak observed at $\delta$ = 4.08 ppm corresponds to the enolic OH group in the compound, which was found to undergo exchange on addition of $D_2O$, thus confirming the existence of this compound in the enolic form. The absence of a peak at $\delta$ = 3.8 ppm corresponding to the methylene proton at position 4 of the isoxazolone ring further confirms the existence of HTPI quantitatively in the enolic form. IR: $\tilde{\nu}$ = 2600, 1706, 1613, 1600, 830 cm$^{-1}$. $C_{17}H_{13}NO_3$ (279): calcd. C 73.12, H 4.66, N 5.02; found C 73.52, H 4.73, N 5.31.

**[Eu(TPI)$_3$·3H$_2$O] (1):** An aqueous solution of $Eu(NO_3)_3·6H_2O$ (0.5 mmol) was added to a solution of HTPI (1.5 mmol) in ethanol in the presence of NaOH (1.5 mmol). Precipitation took place immediately and the reaction mixture was stirred at room temperature for 10 h (Scheme 2). It was then filtered, washed with ethanol, water and then with ethanol, and dried and stored in a desiccator. $C_{51}H_{42}EuN_3O_{12}$ (1040.0): calcd. C 58.84, H 4.04, Eu 14.61, N 4.04; found C 58.63, H 4.27, Eu 14.59, N 4.4. IR (KBr): $\tilde{\nu}_{max}$ = 3300, 2919, 1640, 1606, 1441, 1387, 1189, 917, 771 cm$^{-1}$.

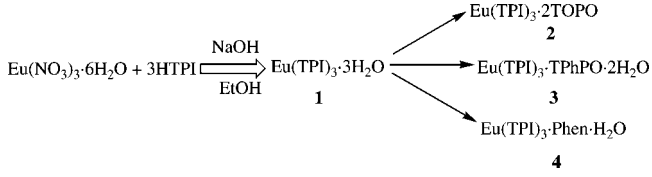


Scheme 2.

**[Eu(TPI)$_3$·2TOPO] (2):** An aqueous solution of $Eu(NO_3)_3·6H_2O$ (0.5 mmol) was added to a mixture of HTPI (1.5 mmol) and TOPO (1.0 mmol) in ethanol in the presence of NaOH (1.5 mmol). Precipitation took place immediately and the reaction mixture was stirred at room temperature for 10 h (Scheme 2). It was then filtered, washed with ethanol, water and then with ethanol, dried, and stored in a desiccator.$C_{99}H_{138}EuN_3O_{11}P_2$ (1759.3): calcd. C 67.53, H 7.84, Eu 8.64, N 2.39; found C 67.57, H 8.16, Eu 8.61, N 2.59. IR (KBr): $\tilde{\nu}_{max}$ = 2925, 2839, 1643, 1603, 1570, 1483, 1380, 1132, 909, 767 cm$^{-1}$.

**[Eu(TPI)$_3$·TPhPO·2H$_2$O] (3):** An aqueous solution of $Eu(NO_3)_3·6H_2O$ (0.25 mmol) was added to a mixture of HTPI (0.75 mmol) and TPhPO (0.5 mmol) in ethanol in the presence of NaOH (0.75 mmol). Precipitation took place immediately and the reaction mixture was stirred at room temperature for 10 h (Scheme 2). It was then filtered, washed with ethanol, water and then with ethanol, dried, and stored in a desiccator.$C_{69}H_{55}EuN_3PO_{12}$ (1300.3): calcd. C 63.67, H 4.23, Eu 11.68, N 3.23; found C 63.69, H 3.64, Eu 11.64, N 3.44. IR (KBr): $\tilde{\nu}_{max}$ = 3400, 2912, 2853, 1679, 1640, 1606, 1480, 1381, 1155, 910, 771 cm$^{-1}$.

**[Eu(TPI)$_3$·Phen·H$_2$O] (4):** An aqueous solution of $Eu(NO_3)_3·6H_2O$ (0.5 mmol) was added to a mixture of HTPI (1.5 mmol) and 1,10-phenanthroline (0.5 mmol) in ethanol in the presence of NaOH (1.5 mmol). Precipitation took place immediately and the reaction mixture was stirred at room temperature for 10 h (Scheme 2). It was then filtered, washed with ethanol, water and then with ethanol, dried, and stored in a desiccator. $C_{63}H_{46}EuN_5O_{10}$ (1184.2): calcd. C 63.84, H 3.88, Eu 12.83, N 5.91; found C 64.08, H 3.92, Eu 12.80, N 5.09. IR (KBr): $\tilde{\nu}_{max}$ = 3402, 2919, 1639, 1608, 1574, 1476, 1445, 1384, 1180, 916, 844, 766 cm$^{-1}$.

 © 2005 Wiley-VCH Verlag GmbH & Co. KGaA, Weinheim 

## Acknowledgments

The authors would like to acknowledge the financial support from the Council of Scientific and Industrial Research and Defence Research and Development Organization, India. The authors also wish to thank Prof. T. K. Chandrashekar, Director, Regional Research Laboratory, Trivandrum, for constant encouragement. The authors acknowledge CNPq, CAPES, FACEPE (Brazilian agencies), PRONEX, PROFIX, Instituto do Milênio de Materiais Complexos, and Programa Primeiros Projetos for financial support, and CENAPAD (Brazilian institution) for providing the computational facilities.

[1] J. Kido, Y. Okamoto, *Chem. Rev.* **2002**, *102*, 2357–2368.
[2] Y. Hasegawa, Y. Wada, S. Yanagida, *J. Photochem. Photobiol. C: Photochem. Rev.* **2004**, *5*, 183–202.
[3] T. Justel, H. Nikol, C. Ronda, *Angew. Chem. Int. Ed.* **1998**, *37*, 3084–3103.
[4] P. Caravan, J. J. Ellison, T. J. McMurry, R. B. Lauffer, *Chem. Rev.* **1999**, *99*, 2293–2352.
[5] D. Parker, *Coord. Chem. Rev.* **2000**, *205*, 109–130.
[6] J. C. G. Bünzli, C. Piguet, *Chem. Rev.* **2002**, *102*, 1897–1928.
[7] Y. Hasegawa, M. Yamamuro, Y. Wada, N. Kanehisa, Y. Kai, S. Yanagida, *J. Phys. Chem. A* **2003**, *107*, 1697–1702.
[8] N. Sabbatini, M. Guardigli, J. M. Lehn, *Coord. Chem. Rev.* **1993**, *123*, 201–228.
[9] G. F. de Sa, O. L. Malta, C. de Mello Donegá, A. M. Simas, R. L. Longo, P. A. Santa-Cruz, E. F. da Silva, Jr., *Coord. Chem. Rev.* **2000**, *196*, 165–195.
[10] A. Bellusci, G. Barberio, A. Crispini, M. Ghedini, M. La Deda, D. Pucci, *Inorg. Chem.* **2005**, *44*, 1818–1825.
[11] C. de Mello Donegá, S. J. L. Ribeiro, R. R. Gonçalves, G. Blasse, *J. Phys. Chem. Solids* **1996**, *57*, 1727–1734.
[12] C. de Mello Donegá, S. A. Junior, G. F. de Sa, *Chem. Commun.* **1996**, 1199–1200.
[13] R. Pavithran, M. L. P. Reddy, *Radiochim. Acta* **2004**, *92*, 31–38.
[14] R. O. Freire, G. B. Rocha, A. M. Simas, *Inorg. Chem.* **2005**, *44*, 3299–3310.
[15] J. J. P. Stewart, *MOPAC 93.00 Manual*, Fujitsu Limited: Tokyo, Japan, **1993**.
[16] G. B. Rocha, R. O. Freire, N. B. da Costa, Jr., G. F. de Sa, A. M. Simas, *Inorg. Chem.* **2004**, *43*, 2346–2354.
[17] A. V. M. Andrade, N. B. da Costa, Jr., A. M. Simas, G. F. de Sa, *Chem. Phys. Lett.* **1994**, *227*, 349–353.
[18] J. E. Ridley, M. C. Zerner, *Theor. Chim. Acta* **1976**, *42*, 223–236.
[19] M. C. Zerner, G. H. Loew, R. F. Kirchner, U. T. Mueller-Westerhoff, *J. Am. Chem. Soc.* **1980**, *102*, 589–599.
[20] M. C. Zerner, *ZINDO manual*, **1990**, QTP, University of Florida, Gainesville, FL. 32611.
[21] W. T. Carnall, H. M. Crosswhite, *Energy levels, Structure and Transition Probabilities of the Trivalent Lanthanides in $LaF_3$*, Argonne National Laboratory Illinois, **1977**.
[22] O. L. Malta, F. R. Gonçalves e Silva, *Spectrochim. Acta A* **1998**, *54*, 1593–1599.
[23] O. L. Malta, F. R. Gonçalves e Silva, R. Longo, *Chem. Phys. Lett.* **1999**, *307*, 518–526.
[24] B. R. Judd, *Operator Techniques in Atomic Spectroscopy*, 2nd ed., McGraw-Hill Book Company, New York, USA, **1998**.
[25] O. L. Malta, H. F. Brito, J. F. S. Menezes, F. R. Gonçalves e Silva, S. Alves, Jr., F. S. Farias, Jr., A. M. V. de Andrade, *J. Lumin.* **1997**, *75*, 255–268.
[26] C. Pettinari, F. Marchetti, A. Cingolann, A. Drozdov, I. Timokhin, S. I. Troyanov, V. Tsaryuk, V. Zolin, *Inorg. Chim. Acta* **2004**, *357*, 4181–4190.
[27] D. Zhou, Q. Li, C. H. Huang, G. Yao, S. Umetani, M. Matsui, L. Ying, A. Yu, X. Zhao, *Polyhedron* **1997**, *16*, 1381–1389.
[28] J. Yu, L. Zhou, H. Zhang, Y. Zheng, H. Li, R. Deng, Z. Peng, Z. Li, *Inorg. Chem.* **2005**, *44*, 1611–1618.
[29] N. Sabbatini, M. Guardigli, I. Manet, in *Handbook on the Physics and Chemistry of Rare Earths, 21* (Eds.: K. A. Gschneidner, Jr., L. Eyring), Elsevier Science B. V., North Holland, **1996**, p. 69–119.
[30] O. L. Malta, M. A. C. dos Santos, L. C. Thompson, N. K. Ito, *J. Lumin.* **1996**, *69*, 77–84.
[31] O. L. Malta, H. F. Brito, J. F. S. Menezes, F. R. Gonçalves e Silva, S. Alves, Jr., F. S. Farias, Jr., A. V. M. de Andrade, *J. Lumin.* **1997**, *75*, 255–268.
[32] B. R. Judd, *Phys. Rev.* **1962**, *127*, 750–761.
[33] R. D. Peacock, *Struct. Bond.* **1975**, *22*, 83–121.
[34] R. Reisfeld, C. K. Jørgensen, in *Handbook on the Physics and Chemistry of Rare Earths* (Eds.: K. A. Gschneidner, Jr., L. Eyring), Elsevier Science B. V., North Holland, **1987**, chapter 58.
[35] C. de Mello Donegá, S. Alves, Jr., G. F. de Sá, *J. Alloys Compd.* **1997**, *250*, 422– 426.
[36] O. L. Malta, *J. Lumin.* **1997**, *71*, 229–236.

Received: May 20, 2005
Published Online: September 12, 2005

 © 2005 Wiley-VCH Verlag GmbH & Co. KGaA, Weinheim 